



# Reactive-transport modelling of C, N, and O<sub>2</sub> in a river–estuarine–coastal zone system: Application to the Scheldt estuary

Jean-Pierre Vanderborght <sup>a,\*</sup>, Inge M. Folmer <sup>a,b</sup>, David R. Aguilera <sup>b</sup>,  
Thomas Uhrenholdt <sup>c</sup>, Pierre Regnier <sup>b</sup>

<sup>a</sup> *Laboratory of Chemical Oceanography and Water Geochemistry, Université Libre de Bruxelles, CP 208, Bd du Triomphe, B-1050 Brussels, Belgium*

<sup>b</sup> *Department of Earth Sciences - Geochemistry, Faculty of Geosciences, Utrecht University, P.O. Box 80.021, NL 3508 TA Utrecht, The Netherlands*

<sup>c</sup> *DHI Water and Environment, Artens Allé 5, DK-2970 Horsholm, Denmark*

Received 22 December 2005; received in revised form 15 May 2006; accepted 14 June 2006

## Abstract

A fully coupled, two-dimensional hydrodynamic and reactive-transport model of C, N, O<sub>2</sub> and Si along a river–estuarine–coastal zone system is presented. It is applied to the Scheldt continuum, a macrotidal environment strongly affected by anthropogenic perturbations. The model extends from the upper tidal river and its tributaries to the southern Bight of the North Sea. Five dynamically linked nested grids are used, with a spatial resolution progressively increasing from 33 m to 2.7 km. The biogeochemical reaction network consists of aerobic degradation, nitrification, denitrification, phytoplankton growth and mortality, as well as reaeration. Diagnostic simulations of a typical summer situation in the early 1990s are compared to field data taken from the OMES database (>300 samples per variable). Results demonstrate that the process rates in the tidal river are very high and far larger than in the saline estuary, with maximum nitrification rates in the water column up to 70 mM N day<sup>−1</sup>, and maximum aerobic respiration and denitrification up to 70 and 40 mM C day<sup>−1</sup>, respectively. Phytoplankton production is about one order of magnitude lower, a result which confirms the dominance of heterotrophic processes in this system. The influence of secondary and tertiary wastewater treatment in the catchment is then assessed. Results show a significant decrease of organic matter and ammonium concentrations above Antwerp, which in turn leads to a partial restoration of oxygen levels. The model also predicts a reduction of denitrification rates, which locally results in a 4-fold increase of the nitrate concentration. Mass budgets for carbon, nitrogen and oxygen are established for the saline estuary (km 0 to 100) and for the tidal river network (km 100 to 160). Three scenarios, corresponding to the situation in the early 1990s, the years 2000 and the situation expected in 2010 are considered. They show that the tidal river and the estuary contribute almost equally to the overall biogeochemical cycling of these elements, despite the very different water volumes involved. For the simulated periods, the large decrease in nitrogen input (>55%) expected between 1990 and 2010 will not lead to a significant decrease of N export to the coastal zone during the summer period.  
© 2006 Elsevier B.V. All rights reserved.

**Keywords:** Estuaries; Biogeochemistry; Modelling; Nutrients; Estuarine dynamics; Brackishwater pollution; Scheldt

\* Corresponding author. Fax: +32 2 650 5228.

E-mail address: [vdborght@ulb.ac.be](mailto:vdborght@ulb.ac.be) (J.-P. Vanderborght).

## 1. Introduction

The crucial role of estuaries in the transfer of land-derived material to the marine system is now fully recognized, and the biogeochemical processes occurring in these environments are studied with increasing attention (Wollast, 2003). This is largely due to the growing impact of anthropogenic activities that have profoundly affected the quality of fresh and marine waters over the last 50 years. In coastal seas, such alterations are well documented and have been linked to perturbations in nutrient export fluxes from the continent (Lancelot et al., 1997). Yet, the quantitative evaluation of these fluxes remains challenging, particularly when reactive constituents transit through the river–estuarine continuum, where intense physical, chemical and biological transformations may occur (Tappin et al., 2003).

The net exchange of nutrients between the estuary and the coastal zone can be evaluated from an inventory of riverine input and an estimation of the production/removal of these nutrients within the continuum. The direct estimate of net fluxes at the estuarine mouth constitutes an alternative approach, but it is particularly challenging in macrotidal estuaries, where the residual material fluxes are several orders of magnitude smaller than the tidal, instantaneous fluxes (Jay et al., 1997; Regnier et al., 1998). It is therefore generally accepted that modelling is a particularly useful method for the evaluation of estuarine fluxes. Several approaches exist and include, in order of increasing complexity, property–salinity plot analysis, mass balances and budgets estimations, steady-state box modelling and, finally, transient reactive-transport approaches (for a recent review, see Tappin, 2002). The latter often rely on an explicit computation of the flow field based on mass and momentum conservation equations.

The weaknesses of the former three modelling approaches have already been comprehensively documented in the literature (Officer and Lynch, 1981; Loder and Reichard, 1981; Regnier et al., 1998; Regnier and O’Kane, 2004). Yet, despite obvious flaws in these methods, they are still used by international agencies and regulatory authorities, in particular in the framework of the LOICZ program. The recent development of Reactive-Transport Models (RTMs) for estuarine systems, which provide a mechanistic, process-based understanding of nutrient dynamics at a coherent spatial and temporal scale, constitutes an interesting alternative. Such models incorporate transient and non-linear properties in both the flow and concentration fields whose effects may seriously influence nutrient flux

estimations (Jay et al., 1997; Regnier and Steefel, 1999; Tappin, 2002). Currently, the few existing RTMs that include a comprehensive set of state variables and reactions for the simulation of nutrient dynamics in estuaries have mostly been limited to one-dimensional (longitudinal) applications (e.g. Lebo and Sharp, 1992; Thouvenin et al., 1994; Soetaert and Herman, 1995a,b; Regnier et al., 1997; Vanderborght et al., 2002; Tappin et al., 2003). Furthermore, the span of such simulations is often restricted to the saline estuary, that is, the zone where significant longitudinal chlorinity gradients are observed. Prognosis and scenario of reduced anthropogenic perturbations require nevertheless to be performed within comprehensive models of the whole aquatic continuum, from the catchment to the coastal zone. Models of interconnected compartments of the hydrosphere point the way to future developments and, to our knowledge, have so far only been implemented in the case of the Seine (Garnier et al., 1995; Billen et al., 2001) and Humber continuums (Proctor et al., 2000; Tappin et al., 2003). In order to be numerically tractable, simulations of such large-scale systems have exclusively been performed at a relatively low spatial and temporal scale of resolution, using significant dynamical approximations in the physics.

The present work is a first attempt to develop a fully coupled two-dimensional, hydrodynamic and reactive-transport model of C, N, O<sub>2</sub> and Si dynamics along a river–estuary–coastal zone system under strong tidal influence. A variable resolution of the physical support is proposed, where the spatial grid of the model is adapted to the local geometrical characteristics. Such methodology is particularly useful in the framework of the continuum approach, where length scales typically vary over several orders of magnitude, from 10<sup>2</sup> m in the tidal rivers to 10<sup>4</sup> m in the coastal zone. With this approach, small-scale topographical features can be resolved. At the same time, the large geographical extension of the physical support allows to compute mass fluxes through the interfaces between these system’s compartments.

The model is developed within the MIKE 21-ECO Lab simulation environment. It is particularly suitable for the implementation of alternative reaction networks and process formulations of increasing complexity. The model is applied to the Scheldt estuary (Belgium–The Netherlands) as an example. Its performance in terms of hydrodynamics, transport and biogeochemistry is first evaluated using a comprehensive data set of the riverine and estuarine zones for the early 1990s. Scenarios of wastewater purification are then run for both the present-day situation and the year 2010 when the last large-scale pollution point sources within the catchment will be

removed. The scenarios are compared in terms of concentration profiles and rate distributions along the continuum. The change in heterotrophic status of the estuary over the years is then analyzed based on the evolution in relative biogeochemical process intensities. Finally, mass budgets and fluxes in the river and estuarine portions of the continuum are presented for C, N and O<sub>2</sub>.

## 2. The Scheldt estuary

The Scheldt River and its tributaries drain 21,580 km<sup>2</sup> in northwestern France, northern Belgium and southwestern Netherlands (Fig. 1). The tidal regime is semi-diurnal with mean neap and spring ranges of 2.7 and 4.5 m, respectively. The average freshwater discharge is close to 100 m<sup>3</sup> s<sup>-1</sup>, which represents 4.8×10<sup>6</sup> m<sup>3</sup> during one M<sub>2</sub> tidal period, while the volume of sea water entering the estuary during the flood is about 1×10<sup>9</sup> m<sup>3</sup> (Peters and Sterling, 1976; Wollast, 1988). The Scheldt estuary is therefore considered as a macrotidal system, with an average residence time in brackish waters of 1 to 3 months. The mixing zone of fresh and salt waters extends over a distance of 70 to 100 km. The area of tidal influence goes up to 160 km from the river mouth and includes all the major tributaries.

On the basis of geometrical and dynamical criteria, the Scheldt estuary can be divided into three zones (Peters and Sterling, 1976). The first zone, between the estuarine mouth and Waalsoorden (km 45), is characterized by a complicated system of ebb and flood channels. The tidal motion is large and mixing is important. From Waalsoorden to Rupelmonde (km 103), the estuary

reduces to a single, well-defined channel in which mixing is partial, with large longitudinal and small vertical salinity gradients being observed during a tidal cycle. The third zone above km 100 constitutes the tidal river and includes a complex network of 6 tributaries (Dender, Durme, Grote Nete, Kleine Nete, Zenne and Dijle rivers, see Fig. 2). The latter four form together the Rupel, a single stream of about 10 km length which flows into the Scheldt estuary at km 103, an area which corresponds roughly to the limit of the salt intrusion.

The hydrographical basin includes one of the most heavily populated regions of Europe, where highly diversified industrial activity has developed. As a consequence, the whole catchment has been heavily polluted until the mid 1970s, when water degradation culminated due to the continuous increase of nutrient and organic matter inputs. The low level of wastewater treatment, especially in the upstream zones, was an important factor contributing to this degradation. The estuary was particularly affected by domestic and industrial inputs from the great Brussels, Antwerp and Gent areas. Since then, better management of industrial and domestic wastewater point sources has led to a progressive improvement of the environmental conditions in the estuary. Billen et al. (2005) and Soetaert et al. (2006) provide two recent comprehensive reviews of this long-term evolution.

## 3. Model set-up

### 3.1. Support

A two-dimensional, vertically integrated model (MIKE 21, [www.dhisoftware.com/mike21](http://www.dhisoftware.com/mike21)) is used to

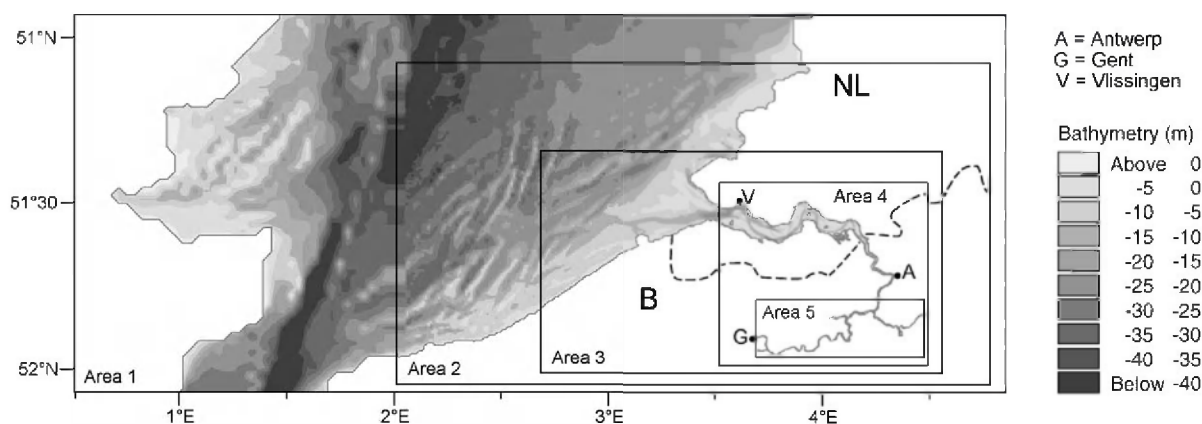


Fig. 1. Geographical extension of the nested-grid model. The finest grid includes the tidal rivers with a resolution of 33×33 m (area 5); the estuary is described with a coarser grid of 100×100 m (area 4) and the coastal zone with three different resolutions of 300×300 m, 900×900 m and 2700×2700 m (areas 3 to 1). Levels are given with respect to Mean Low Low Water Spring (MLLWS) at Vlissingen. Origin of the grid (lower right corner): 50°54'30"N–0°28'42"E.

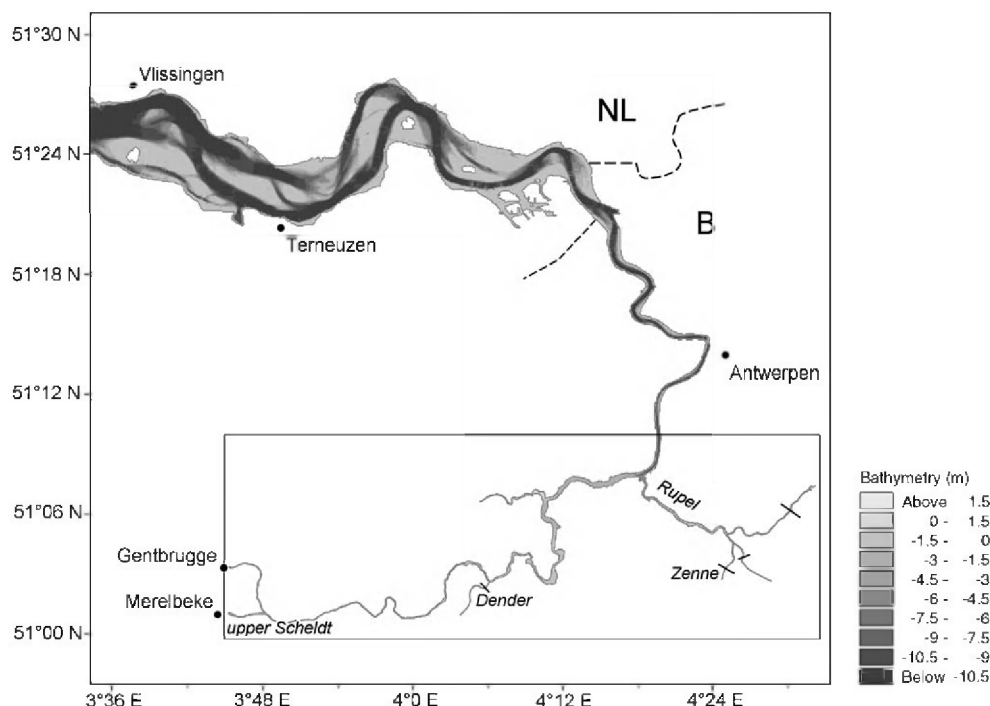


Fig. 2. Bathymetric map of the Scheldt estuary and the tidal rivers (areas 4 and 5). Levels are given with respect to MLLWS at Vlissingen. Useful distances to the mouth: Vlissingen: 2 km, Walsoorden: 45 km, Antwerpen: 90 km, Rupelmonde: 103 km, Appels: 141 km, Merelbeke: 167 km.

resolve the longitudinal and transverse hydrodynamic flows in the estuary, which arise from the complex topography of the Western Scheldt (Figs. 1 and 2). Scaling analysis of the three-dimensional Navier–Stokes equations shows that the along-channel vertical salinity gradients in the Scheldt can be neglected in the momentum balance (Regnier, 1997). The model extends from the upper tributaries of the Scheldt estuary to the Southern Bight of the North Sea. It includes the river system of the Scheldt, up to the limit of tidal influence where unidirectional flow is maintained at all times, either naturally or by the presence of sluices. Accordingly, the Rupel and its river network, which encompasses the main tributaries with the exception of the Dender, are implemented in the model. The largest distance to the tidal Scheldt is about 25 km. For the Scheldt, the sluices located at Gentbrugge and Merelbeke (Fig. 2) limit the propagation of the tidal wave. Freshwater from the upper Scheldt enters our model domain through the latter location only. The marine area is comprised between latitude 50°54′30″N and 52°03′N.

The model consists of five dynamically linked nested grids. Each nested area is characterized by a spatial resolution which is constrained by the local geometrical features that are important to resolve. Therefore, the

grid size of the numerical model gradually increases in five steps from 33 × 33 m for the tidal rivers (area 5), to 2700 × 2700 m for the Southern Bight of the North Sea (area 1, Fig. 1). For area 1, 2 and part of area 3, the land boundaries and the bathymetry are taken from the C-Map digital charts using the MIKE C-Map extraction tool ([www.dhisoftware.com/mikecmap](http://www.dhisoftware.com/mikecmap)). For the remaining part of the outer estuary in area 3 and for area 4, the information is obtained from the navigational charts edited by the Coastal Hydrographical Service of the Flemish authorities (AWZ, 2003). Finally, the topographic maps of the Belgian National Geographic Institute have been used for area 5, where an estimated bottom slope has only been implemented in the model.

### 3.2. Hydrodynamics

The hydrodynamic model is based on the vertically integrated volume and momentum conservation equations for barotropic flow, which read:

– for volume conservation:

$$\frac{\partial \zeta}{\partial t} + \frac{\partial p}{\partial x} + \frac{\partial q}{\partial y} = 0 \quad (1)$$



– for the  $X$ - and  $Y$ -components of the momentum equation:

$$\frac{\partial p}{\partial t} + \frac{\partial}{\partial x} \left( \frac{p^2}{h} \right) + \frac{\partial}{\partial y} \left( \frac{pq}{h} \right) + gh \frac{\partial \zeta}{\partial x} + gp \sqrt{\frac{p^2 + q^2}{C^2 h^2}} \left[ E_x \frac{\partial^2 p}{\partial x^2} + E_y \frac{\partial^2 p}{\partial y^2} \right] - \Omega q = 0 \quad (2)$$

$$\frac{\partial p}{\partial t} + \frac{\partial}{\partial y} \left( \frac{q^2}{h} \right) + \frac{\partial}{\partial x} \left( \frac{pq}{h} \right) + gh \frac{\partial \zeta}{\partial y} + gp \sqrt{\frac{p^2 + q^2}{C^2 h^2}} \left[ E_x \frac{\partial^2 q}{\partial y^2} + E_y \frac{\partial^2 q}{\partial x^2} \right] - \Omega p = 0 \quad (3)$$

All variables and parameters used in Eqs. (1), (2) and (3), along with their associated units, are defined in Table 1. This set of coupled non-linear partial differential equations (PDEs) provides the temporal evolution in surface water elevations,  $\zeta$ , and scalar components of the momentum fluxes,  $p$  and  $q$ , over the whole domain. Effects of wind stress and variations of the barometric pressure are not considered in the present version of the hydrodynamic model. Flux densities  $p$  and  $q$  are defined per unit length along the  $y$  and  $x$  coordinates, respectively.

The system of PDEs is solved with appropriate initial and boundary conditions by finite differences, using the non-iterative alternating direction implicit algorithm (Abbott, 1979). Manning–Strickler and eddy viscosity coefficients are model parameters that must be specified.

### 3.2.1. Boundary conditions

Water elevations are provided in the outer grid at the northern and southern limits of the Southern Bight of the North Sea (Fig. 1). These elevations are computed by a large-scale, three-dimensional water forecast model of the whole North Sea and part of the Atlantic Ocean (Jensen et al., 2002). Constant river discharges are specified at the continental limits of the model, for the Scheldt River and all its tributaries (Table 2). For the simulated period considered here, the selected, constant

Table 1  
Variables, constants and parameters of the hydrodynamic equations

Name	Definition	Units
$t$	Time	s
$x, y$	Spatial (horizontal) coordinates	m
$\zeta$	Surface elevation	m
$p, q$	Flux densities	$\text{m}^3 \text{s}^{-1} \text{m}^{-1}$
$h$	Water depth	m
$g$	Gravity constant	$\text{m s}^{-2}$
$\Omega$	Coriolis parameter	$\text{s}^{-1}$
$C$	Chezy coefficient	$\text{m}^{1/2} \text{s}^{-1}$
$E_x, E_y$	Eddy viscosity coefficients	$\text{m}^2 \text{s}^{-1}$

Table 2  
River discharge selected for the simulations

River	Discharge ( $\text{m}^3 \text{s}^{-1}$ )
Upper Scheldt River	32
Dender	4.1
Dijle	17.8
Zenne	6.6
Grote Nete	3.5
Kleine Nete	4.8

Total freshwater discharge amounts to  $69 \text{ m}^3 \text{s}^{-1}$ . (Source of data: Ministry of the Flemish Community, Department “Maritieme Scheldt”).

freshwater flows are representative of an average summer situation.

### 3.2.2. Model parameters

Eddy viscosity coefficients are computed from local current velocities using the Smagorinsky (1963) formula with a proportionality constant of 0.5. The Manning–Strickler coefficient  $M [\text{m}^{1/3} \text{s}^{-1}]$ , that is, the reciprocal of the Manning roughness, has been used to constrain the bed friction. It is related to the Chezy coefficient according to  $C = Mh^{1/6}$ . A Manning–Strickler coefficient of 32 has been used in all areas, except for the estuary where it is set to 50.

### 3.3. Transport

The transport and biogeochemical models are based on the vertically integrated advection–dispersion equation:

$$\frac{\partial}{\partial t} (hc) + \frac{\partial}{\partial x} (uhc) + \frac{\partial}{\partial y} (vhc) - \frac{\partial}{\partial x} \left( h D_x \frac{\partial c}{\partial x} \right) - \frac{\partial}{\partial y} \left( h D_y \frac{\partial c}{\partial y} \right) - Q_s (c_s - c) - R = 0 \quad (4)$$

where  $c$  is the species concentration [ $\text{mol m}^{-3}$ ],  $u = p/h$  and  $v = q/h$  are the horizontal components of the velocity vector [ $\text{m s}^{-1}$ ],  $D_x$  and  $D_y$  are the dispersion coefficients [ $\text{m}^2 \text{s}^{-1}$ ] and  $Q_s$  represents sink/source discharges [ $\text{m}^3 \text{m}^{-2} \text{s}^{-1}$ ] with species concentration  $c_s$ . In Eq. (4),  $R$  is the rate of production ( $R > 0$ ) or consumption ( $R < 0$ ) of the species by biogeochemical processes, defined per unit surface area [ $\text{mol m}^{-2} \text{s}^{-1}$ ]. For salt, both  $Q_s$  and  $R$  are set to zero.

The hydrodynamic model, which is solved separately, provides the horizontal velocity components  $u$  and  $v$  as well as the water depth  $h$  also present in (4). The equation is then solved for the spatial and temporal evolution of the concentration field using appropriate initial and boundary conditions. Numerical discretization of Eq. (4) is performed using the QUICKEST explicit scheme,

which is a third order, finite difference algorithm (Ekebjærg and Justesen, 1991). Both the hydrodynamic and transport models are run with a time step of 15 s to achieve stability of the numerical schemes.

### 3.3.1. Boundary conditions

The salinity is set respectively to 35 at the northern and southern limits of the outer grid, and to 0 at the continental limits of the model domain.

### 3.3.2. Model parameters

The dispersion coefficients  $D_x$  and  $D_y$  in Eq. (4) are model parameters. Their values are given in Table 3 for the five nested areas. The magnitude of the dispersion coefficients reflects the growing influence of sub-grid scale processes when the model grid size is increasing (Fischer et al., 1979).

### 3.4. Biogeochemistry

The reaction network has been implemented in the model by means of the ECO Lab ecological modelling tool ([www.dhisoftware.com/ecolab](http://www.dhisoftware.com/ecolab)). It consists of 6 mass transfer processes acting on 6 state variables (Table 4). This reaction network is described in details and illustrated in Appendix A and is similar to the one already implemented in the most recent version of the 1D CONTRASTE model (Regnier and Steefel, 1999; Vanderborght et al., 2002). With the exception of the kinetic rate constant for nitrification, which has been adjusted during the process of model calibration, all other parameters have been determined independently from field and/or laboratory studies in the Scheldt estuary, performed either *in situ*, or using Scheldt water samples.

In short, we simulate the growth of phytoplankton by photosynthesis, taking into account light and silica limitations. Only diatoms have been considered in the present study, since they are dominant throughout the year in the freshwater and brackish reaches of the estuary (Muylaert et al., 2000). No distinction has been made so far in terms of diatom species composition. Diatom mortality, together with the large organic loads flowing through the boundaries or discharged as lateral

Table 4

Variables and processes implemented in the biogeochemical model

State variables	Processes
Labile organic matter	Aerobic respiration
Oxygen	Phytoplankton production
Ammonium	Phytoplankton mortality
Nitrate	Nitrification
Silica	Denitrification
Diatoms	Oxygen transfer

inputs, supplies the detrital organic matter pool, which decomposes by aerobic degradation and denitrification. Nitrate concentrations are such that no other redox metabolic pathway is active in the water column of the Scheldt. Easily degradable organic matter is only considered here (referred to as “labile organic matter” in what follows). Accordingly, measured or estimated biological oxygen demand (B.O.D.) values have been used to quantify the boundary fluxes and the lateral inputs of this variable. Decaying diatom cells are assumed to be composed of labile material only. In addition, no distinction is currently made between the dissolved and particulate organic fractions. It is therefore assumed that sedimentation does not lead to a significant short-term accumulation of labile organic matter within the system. Nitrification is another process controlling nitrogen speciation and oxygen levels. The latter is also influenced by gas exchange at the air–water interface.

In order to limit computational time, an approximate analytical solution for depth-integrated primary production has been implemented in the model (Appendix B). Another difference with respect to the former CONTRASTE model (Regnier et al., 1997; Regnier and Steefel, 1999; Vanderborght et al., 2002) is the incorporation of silica as an explicit state variable.

### 3.4.1. Initial and boundary conditions

Fixed concentrations are imposed at the northern and southern boundaries of the outer grid in the North Sea. Fixed concentrations are also imposed for all tributaries at the continental limits of the model area. Initial concentrations are either taken as the average between upper and lower boundary values, or obtained from the results of a former model run. In all cases, the simulated period extends over one month to guarantee that quasi steady state is achieved. Model results always correspond to the last day(s) of the simulation.

## 4. Diagnostic simulations

For the purpose of model validation, the selection of the most appropriate time period depends on the

Table 3

Dispersion coefficients selected for the transport model

Area and grid size (m)	Dispersion coefficient ( $\text{m}^2 \text{s}^{-1}$ )
1 (2700 × 2700)	1350
2 (900 × 900)	450
3 (300 × 300)	150
4 (100 × 100)	100
5 (33 × 33)	4

availability of reliable field data, both in terms of inputs (freshwater flow, composition of tributaries, lateral loads) and of resulting concentrations of chemical species within the entire system. Coherent and complete data sets are available for the modelled domain since the 1990s only, although it is known from field observation that water degradation in the Scheldt estuary was at its worst in the early 1970s (Van Damme et al., 1995). The focus of the diagnostic simulations has thus been restricted to the situation prevailing in the early 1990s. Within this period (labelled “1990” in what follows), the selected summer seasons correspond to the situation during which the transformation processes are the most active. Table 5 gives the concentration values at the upper boundaries, together with the lateral input fluxes as specified in the SAWES database (1991). These lateral inputs have been distributed along the Scheldt continuum, using the 16-box subdivision of the MOSES model (Soetaert and Herman, 1995a,b). For all simulations, a temperature of 17 °C has been applied. Constant cloud coverage of 58%, corresponding to the mid-year

value in Belgium (IRM, 2004) has been used. The corresponding daily peak solar irradiance varies between 1068 and 1091  $\mu\text{E m}^{-2} \text{s}^{-1}$  for the selected period (15 June–15 July).

Direct comparison between available field measurements and model results is not possible for three main reasons. First, the 2D framework of the simulation does not match the 1D longitudinal labelling of the field data. Second, the sampling during longitudinal surveys is not synoptic with respect to the tide. The latter can easily be resolved in the lower estuary, where salt is a tracer that can be used to recast the data within a synoptic frame (O’Kane and Regnier, 2003); yet this procedure cannot be applied in the freshwater, tidal river. Third, the temporal resolution of freshwater composition time-series which are available to constrain the upstream boundary conditions ( $\sim 1$  week at best) is lower than the intrinsic timescales of both the main (semi-diurnal and diurnal) tidal harmonics and the rapidly fluctuating river discharge. This leads to the well-known phenomenon of temporal aliasing. Accordingly, the comparison between

Table 5

(a) Freshwater flow ( $\text{m}^3 \text{s}^{-1}$ ) and composition ( $\text{mmol m}^{-3}$ ) of the upper Scheldt River (Bovenschedt) and tributaries for the various scenarios

Parameter	Bovenschedt		Dender		Zenne			Dijle		Grote Nete		Kleine Nete	
	1990	2000–2010	1990	2000–2010	1990	2000	2010	1990	2000–2010	1990	2000–2010	1990	2000–2010
Flow	32		4.1		6.6			17.8		3.5		4.8	
O.M.	393	289	2565	213	7869	5500	630	374	191	439	125	176	153
O <sub>2</sub>	106	104	31	190	17	0	0	41	173	160	194	215	232
NH <sub>4</sub> <sup>+</sup>	400	126	1575	127	3327	89	70	300	89	238	30	163	29
NO <sub>3</sub> <sup>-</sup>	198	395	21	179	0	363	152	63	363	64	180	96	139
Dia	50	50	0	30	0	0	0	0	0	0	0	0	0
Si	250	250	250	250	250	250	250	250	250	250	250	250	250

(b) Lateral loads ( $\text{mmol s}^{-1}$ )

Location		Labile O.M.		NH <sub>4</sub> <sup>+</sup>		NO <sub>3</sub> <sup>-</sup>	
Name	km	1990	2000–2010	1990	2000–2010	1990	2000–2010
Vlissingen	2	2247	0	972	0	897	0
Terneuzen	23	7349	0	11511	0	3370	0
Hansweert	34	1356	0	847	0	435	0
Walsoorden	45	571	0	847	0	951	0
Bath	57	143	0	174	0	435	0
Doel	65	2640	0	2442	0	2202	0
Lillo	74	6742	2450	2516	1132	1277	0
Boomke	84	3674	747	2018	530	1767	0
Antwerpen	90	4281	14208	1221	6670	299	0
Kruikebeke	97	6421	3536	2018	1561	639	0
Temse	110	0	2616	0	1068	0	0
Mariekerke	118	0	593	0	199	0	0
Appels	141	0	4444	0	1708	0	0
Wetteren	157	0	1757	0	1123	0	0

O.M. = labile organic matter (in carbon); Dia = phytoplankton carbon. Concentrations are assumed to be identical for 2000 and 2010, except for the river Zenne (downstream of the city of Brussels).

A 0 entry in the table indicates that no data are available to constrain the fluxes.

model results and measurements has been carried out using field data averaged over the period selected for our simulations. Within the set of data comprised between May and September for the years 1990–1995 (taken from the OMES database, Maris et al., 2004), only those characterized by a water temperature in the range 15–19 °C have been used for the averaging.

#### 4.1. Hydrodynamics and transport

The model calibration has been performed by comparing model results with hydrographical data and tide predictions based on harmonic analysis. Water elevations and water fluxes were considered, with focus on the estuarine zone only (area 4). The bed friction coefficient in this area has been calibrated using both the amplitude and the phase lag of the tidal wave. The comparison of model predictions with tidal tables at five stations along the estuarine gradient indicates overall agreement between modelled tides and tabulated values with maximum error in amplitude <7.5% and maximum deviation in phase of 18 min around km 60. Further details about the performance of the hydrodynamic model can be found in Arndt et al. (in press).

The evaluation of the model performance, based on scalar quantities, has been carried out by comparing computed water fluxes integrated over selected cross-sections during the flood and ebb periods with empirical values obtained with the cubature method (WKL, 1966). To assess the quality of the integration, the variation of estuarine volume over one tide (mainly related to the spring–neap oscillation) is also taken into consideration. The latter matches almost perfectly (to a fraction of %) the water balance at Vlissingen (freshwater volume over one tide + integrated flood volume = integrated ebb volume + volume variation). Table 6 shows that the deviation between the cubature method and our estimation is on the order of 10% at locations comprised between km 0 and ~65. In all instances, our model based on recent bathymetric data (2002) predicts slightly higher integrated fluxes, a result which could

Table 6  
Water fluxes through selected cross-sections along the Scheldt estuary

Location	Distance (km)	Tidal volume (ebb–flood) ( $10^6 \text{ m}^3$ )		
		This model	Cubature method	% Deviation
Vlissingen	0	1137–1127	1070–1065	+5.8
Terneuzen	16	769–760	717–712	+7.0
Waarde	38	422–417	362–357	+16.7
Hedwipolder	53	139–137	139–135	<1
Lillo	60	92–90	105–101	–11.6

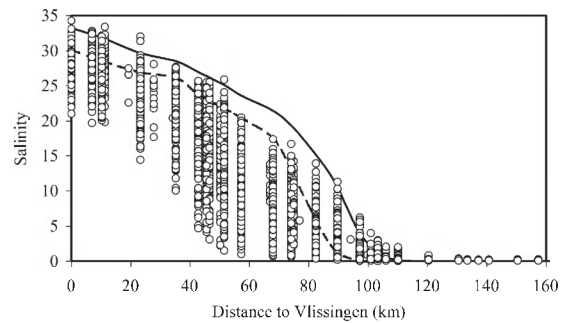


Fig. 3. Envelope of salinity profiles. Field measurements (circles) are reported for the period 1990–2004. Mean (daily) freshwater discharge observed during this period ranged between 26 and 794  $\text{m}^3 \text{s}^{-1}$ . The 2 curves are respectively the minimum (ebb) and maximum (flood) computed values over a neap–spring cycle for a total freshwater discharge of 69  $\text{m}^3 \text{s}^{-1}$ .

partly be explained by the continuous dredging and deepening of the estuarine channels since the 1960s. Note that a significant fraction of the error (~6%) occurs already at the estuarine–coastal zone interface (km 0). Further improvement in the hydrodynamic calibration should thus focus on a better parameterization of tides and currents in the Southern Bight of the North Sea and adjacent coastal zone. This analysis is confirmed by the significant reduction in the error when the model is restricted to the mouth of the Scheldt estuary and forced by an astronomical tide at km 0 (results not shown).

The dispersion coefficients given in Table 3 have been selected using a simple fitting procedure based on salinity profiles. Their magnitude reflects the increasing size of the grid spacing in the seaward direction. Although calibration of dispersive transport using salinity cannot be achieved in the tidal river, the magnitude of dispersion in the upper reaches of the continuum (area 5) is small compared to advective transport and contributes only marginally to the total scalar fluxes in this area. Fig. 3 shows that the envelope of salinity profiles simulated over a tidal cycle using the adjusted set of dispersion coefficients falls within the upper range of observed values, a result consistent with the low discharge conditions used in our simulations.

#### 4.2. Biogeochemistry

Fig. 4 shows the envelope of concentrations simulated over 24 h for oxygen, nitrogen species and silica in the Scheldt River and estuary. These concentration profiles are reported along the longitudinal curvilinear axis following the main navigation channel of the estuary, and are thus not salinity–property plots.



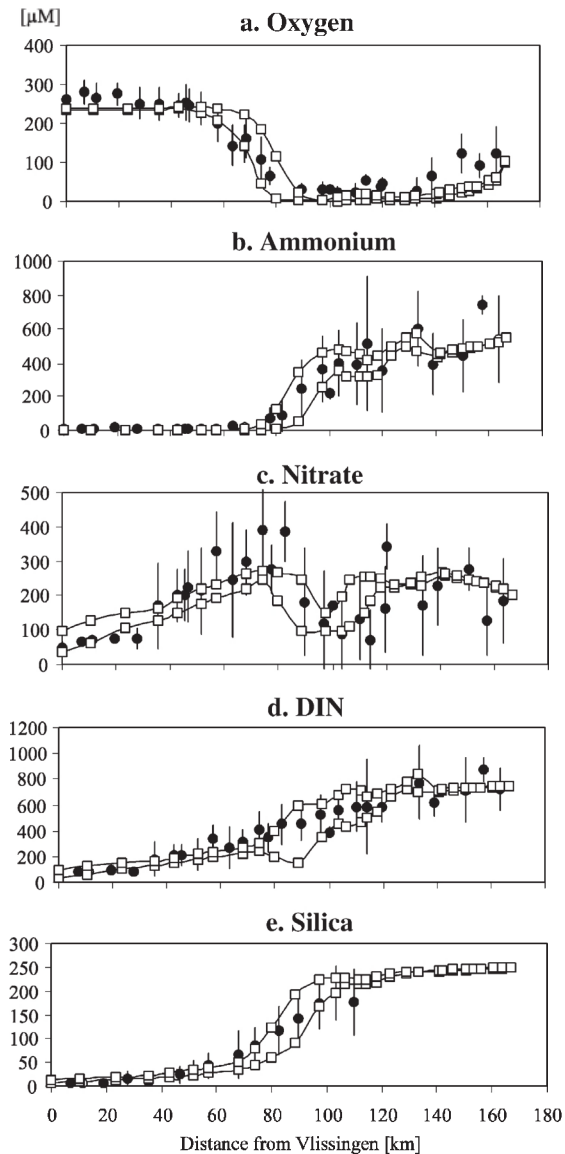


Fig. 4. Comparison between computed longitudinal profiles (open squares, 1990 simulation) and field data (filled circles, mean values for the period 1990–1995) for oxygen, nitrogen and silica. The vertical bars give the standard deviation of the data set. The two lines correspond to the minimum and maximum values reached during the last day (24 h) of our monthly simulation.

Note that the two curves defining the envelope of concentrations in Fig. 4 are generally close to, but not necessarily identical to the conditions at ebb and flood. This discrepancy is due to the complex influence of asynchronous physical forcing (velocity, depth, irradiance, etc.) on transport and reaction mechanisms. Results reported here relate to the last 24 h of our monthly simulation, with no residual influence of the

initial conditions. They correspond to a situation of mean tidal amplitude (about 3.50 m at Vlissingen, as compared to mean spring and neap tide amplitudes of 4.46 and 2.97 m, respectively). The mean concentration values obtained from field data, together with standard deviations (selected according to the criteria described above) are also presented for comparison. All biogeochemical processes incorporated in the reaction network influence, directly or indirectly, the selected state variables, which can thus be used for understanding the system dynamics and for assessing the model performance.

The main trends simulated in the estuarine portion of the transect (km 0 to 90) are consistent with both field data and previous modelling studies (Soetaert and Herman, 1995a; Regnier et al., 1997; Vanderborght et al., 2002) and show: (i) a sharp oxygen gradient in the brackish zone (km 90 to 60), followed by a constant, nearly saturated concentration in the lower Scheldt (Fig. 4a); (ii) an abrupt decrease of ammonium, which leads to an almost complete removal of  $\text{NH}_4^+$  within the uppermost portion of the brackish estuary (km 90 to 80, Fig. 4b); (iii) an increase in nitrate between km 90 and 80, followed by conservative dilution below  $\sim$ km 80 (Fig. 4c). Overall agreement between modelled and observed longitudinal transects of dissolved inorganic nitrogen (DIN) and silica is also satisfactory (Fig. 4d and e).

The extension of the model domain to include the tidal rivers provides new insights into the Scheldt system, which are particularly important for the understanding of the biogeochemical dynamics in the estuarine continuum. Fig. 4a–e shows that model results are in good agreement with available field data in this region. To cast further light on the system dynamics in this portion of the continuum, along-channel distribution of process rates are also presented (Fig. 5a–d). Results demonstrate that the process intensities are overall much larger in the upper reaches of the continuum, km 80 being the limit of an extremely active biogeochemical system. This is mainly the result of the progressive consumption of reactive, reduced species (organic matter and ammonium), combined with the increasing dilution due to the widening and deepening of the estuary. Oxygen consumption (Fig. 5a) is primarily the result of nitrification and, to a lesser extent, of heterotrophic respiration. Phytoplankton net production is only a minor source of oxygen, especially compared to gas exchange with the atmosphere. The latter shows a complex spatial pattern because of the influence of the local hydrodynamic forcing (water depth and current velocity). The net reaction rate, computed from the dynamic balance between these processes, never leads to

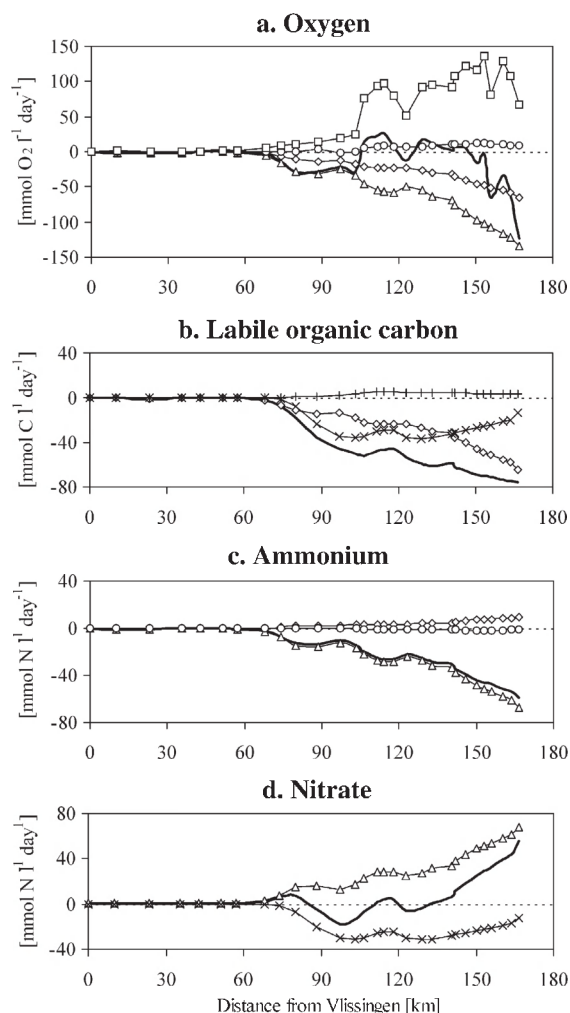


Fig. 5. Along-channel distribution of individual process rates affecting oxygen, organic carbon, ammonium and nitrate ( $\diamond$ =heterotrophic respiration;  $\triangle$ =nitrification;  $\times$ =denitrification;  $\circ$ =NPP;  $+$ =phytoplankton mortality;  $\square$ =gas exchange). The resulting net rate is also presented (thick line).

a significant input of oxygen in the water column. The rapid oxygen restoration observed in the brackish zone (Fig. 4a), where the net rate is still negative, must therefore be attributed to dispersive mixing (Regnier et al., 1997). Fig. 5b shows that aerobic respiration is the dominant metabolic pathway of organic matter degradation between km 170 and km 140. Further down, denitrification becomes dominant until the restoration of oxic conditions around km 80 inhibits this process again. Large lateral inflows of labile organic matter from tributaries (Dender, km 130; Rupel, km 100) contribute to maintain anoxic conditions in the vicinity of their confluence. NPP plays a marginal role in the organic carbon dynamics. The net rate of carbon production/

consumption highlights the heterotrophic dominance of the upper estuary.

Nitrification is by far the dominating process affecting ammonium (Fig. 5c), the contribution from organic matter degradation and NPP in the net rate of  $\text{NH}_4^+$  production/consumption being both much smaller. The ammonium concentration profile (Fig. 4b) shows therefore a continuous decrease in the seaward direction, except when lateral inflows of  $\text{NH}_4^+$ -rich waters from the tributaries (km 100 and 130) alter this longitudinal distribution. Nitrate dynamics results from a complex balance between nitrification and denitrification, the former dominating both in the upstream reach of the system (km 170 to 130) and downstream of km 85 (Fig. 5d). In between, denitrification is the most intense process, which leads to the observed  $\text{NO}_3^-$  sag around km 100.

The benefit of moving the landside model boundaries away from tidal influence can be inferred from concentration time-series simulated at km 100 (Fig. 6). Until now, this area located at the confluence with the Rupel has been selected as the up-estuary limit of most biogeochemical modelling studies (e.g. Wollast, 1978; Billen et al., 1988; Soetaert and Herman, 1995a; Regnier et al., 1997; Regnier and Steefel, 1999; Vanderborcht et al., 2002). Although the highly dynamical pattern illustrated in Fig. 6 could be resolved experimentally using high-frequency data acquisition systems, short-term fluctuations are usually ignored in the design of monitoring programmes. As a result, it is currently impossible to specify realistic boundary conditions at this location. The usefulness of the nested grid approach is also demonstrated by the existence of small-scale spatial variability in process rates. Fig. 7 shows such variability in the case of the distribution of gas exchange

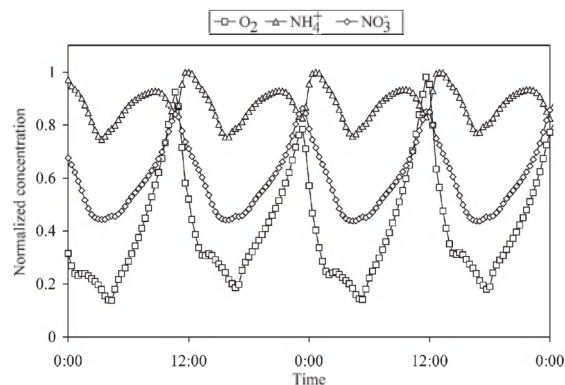


Fig. 6. Concentration time-series computed at km 100 for the 1990 simulation. Values are normalized to maximum concentration observed during for the summer period.

rate in a zone of complex morphology. Our model, despite its large physical extension, resolves this variability and gives therefore some insight on how observational programmes should be designed to minimize experimental errors related to spatial aliasing.

## 5. Scenarios and mass budget

Two additional model runs have been performed to assess the influence of wastewater management policy on the biogeochemistry of the estuary. These simulations aim at reproducing the water quality status corresponding to the present-day (labelled “2000” in what follows) situation, and to forecast the situation for the near future (labelled “2010”). The past and anticipated progress of wastewater treatment in the Scheldt basin has been implemented in the model by changing the boundary conditions only. Their evolution in time mainly reflects (a) the increased secondary and tertiary treatment of domestic wastewater in the catchment during the last decade of the 20th century (<http://www.isc-cie.com>), and (b) the implementation of regional wastewater treatment plants (WTP) for the city of Brussels (<http://www.aquiris.be>). A first WTP, performing secondary treatment for approximately 25% of the population, has been operational since 2000. A second, larger WTP is expected by mid-2007 and should provide secondary and tertiary treatment for the remaining wastewater flow generated within the

Brussels area, which should then comply with the objectives set by the E.U. Urban Wastewater Treatment Directive for the protection of sensitive areas. By the end of the present decade, the last large-scale point source of organic carbon and nutrients in the Scheldt catchment area, which is currently discharging in the river Zenne, should therefore be eliminated.

For the purpose of comparison, the effects of the various wastewater treatment scenarios have been quantified using the same physical forcing conditions and water composition at the marine boundaries as those used for the 1990 simulation. The pollutant loads originating from the upper Scheldt River and the various tributaries differ in the 3 simulations. As for 1990, monitoring data collected in the river network (OMES database) have been used to constrain the loads in the 2000 simulation. For the 2000 and 2010 scenarios, identical lateral inputs have been used, based on data published by the Flemish Environmental Agency (<http://www.vmm.be>). For 2010, an estimate of the water composition in the river Zenne has been carried out based on the expected performance of the WTPs in Brussels. All other river inputs have been left unchanged. Table 5 summarizes the input flows, concentrations and loads selected for the three scenarios. Depending on the catchment areas, inputs of organic carbon and ammonium have been moderately to strongly reduced between 1990 and 2000, reflecting the effect of engineered interventions. However, because

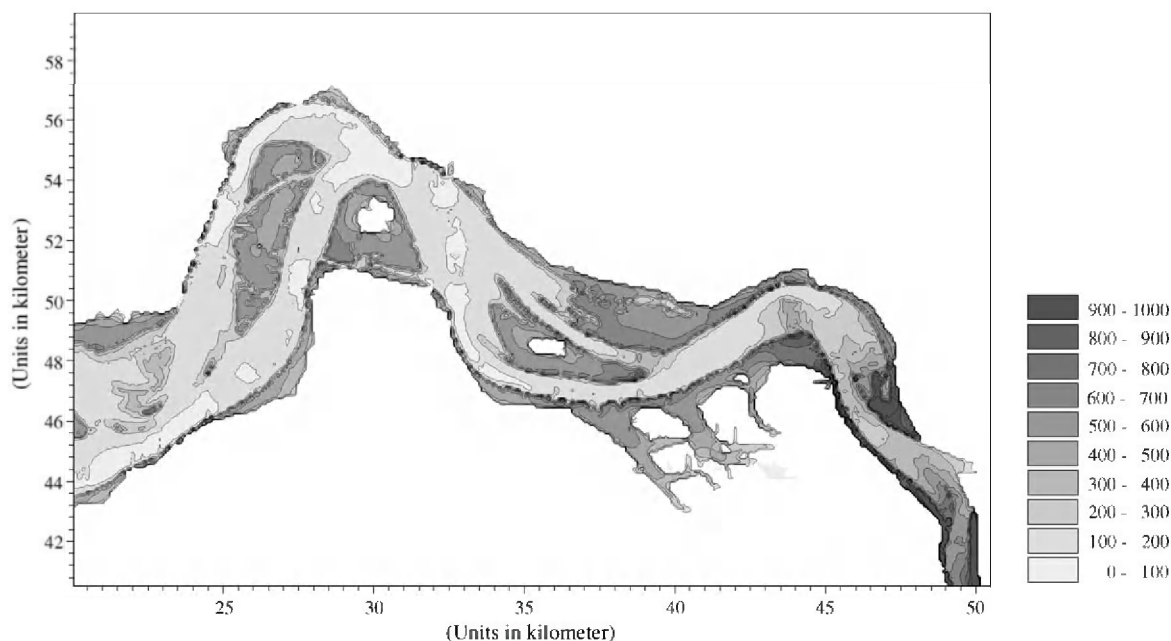


Fig. 7. Snapshot of oxygen exchange rate taken at  $\sim$  mid current velocity. Rate is expressed in  $\text{mol s}^{-1}$  per model grid cell ( $10^4 \text{ m}^2$  for area 4).

tertiary treatment is not generalized in most of the WTPs, the decrease in ammonium is partly compensated by an increase in nitrate. Our estimation assumes a nitrification yield of 90% during biological wastewater treatment and is based on the data from the measurement network of the Flemish region (VMM, 2003). For the 2010 scenario, we only investigate the impact of wastewater treatment in Brussels, assuming that other water quality improvements are of much smaller influence. The latter decreases significantly the organic and inorganic loads discharging into the river Zenne.

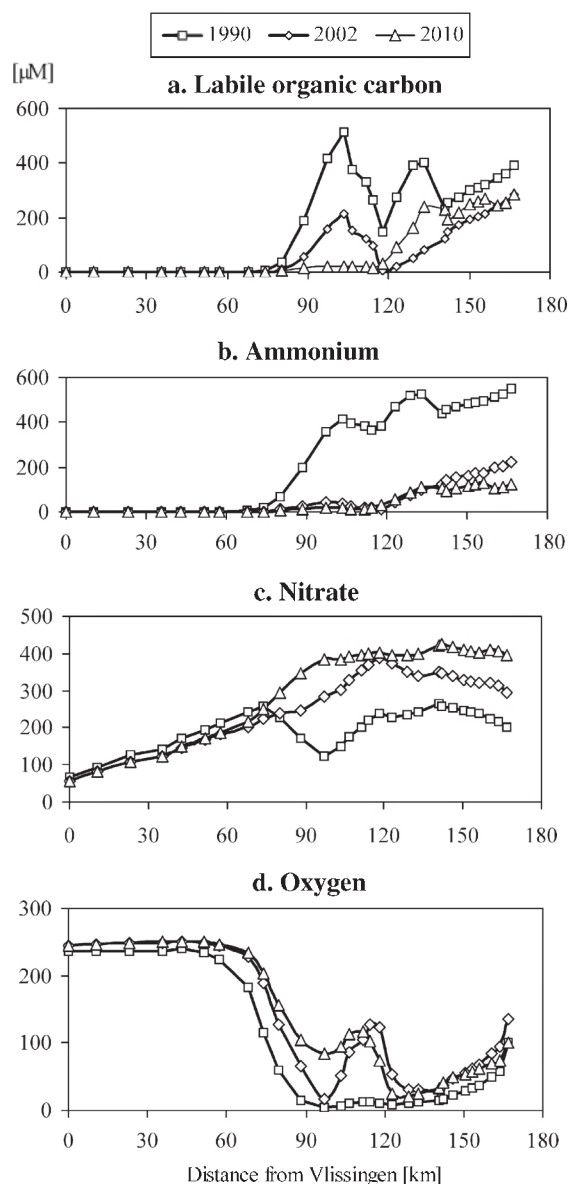


Fig. 8. Longitudinal profiles computed for the 3 model scenarios, showing the effect of changes in load inputs in the catchment.

Fig. 8a–d compares the results of the three 24-h simulations, for (a) labile organic matter, (b) ammonium, (c) nitrate and (d) dissolved oxygen. The organic matter profile (Fig. 8a) is affected by the decrease in organic loads, especially in the up-estuary reach (km 160), and at the confluence with the rivers Dender (km 130) and Rupel (km 100). In particular, the projected situation for 2010 is characterized by a large decrease of the organic matter flux in the Zenne–Rupel system. The simulations illustrate also the purification role of the estuary, as the concentration of labile organic carbon at the mouth remains essentially unaffected by the amount of wastewater treatment performed in the catchment. Only the part of the estuary above the Belgian–Dutch border (km 80) directly benefits from the reduced loads from the city of Brussels. Fig. 8b shows the strong reduction in ammonium concentration since the 1990s, when the release of organic nitrogen and ammonium into the river and estuarine system was only partially controlled. It is expected that lowering the organic matter and ammonium inputs into the system will strongly influence the oxygen demand. This is well illustrated in Fig. 8d, where the improvement of the dissolved oxygen concentration is noticeable along the entire continuum, but is especially striking in the zone under the direct, tidally driven influence of the Rupel (~km 80–120). The increase in nitrate concentrations (Fig. 8c) can be partly attributed to the enhanced release of nitrate by the WTPs, but is also related to the disappearance of an extended anoxic zone in the estuary, and hence, to a large decrease of the denitrification activity, in particular in the vicinity of the city of Antwerp. The local minimum in nitrate concentration, which is predicted at around km 100 in 1990, totally disappears from the longitudinal profiles simulated for 2000 and 2010. The enhanced nitrogen reduction by WTPs is partially compensated by the reduced denitrification within the estuary, as shown by the nitrate concentration profiles between km 70 and the estuarine mouth.

Simulation results are also reported in terms of mass budgets for organic carbon, ammonium, nitrate and oxygen (Fig. 9a–d). Spatial and temporal integration of transformation processes and transport fluxes through boundaries match the mass variation in the system within 0.1%. This indicates that mass conservation is almost perfectly achieved by our model. For the interpretation of the results, the Scheldt continuum has been divided into two different areas: the tidal river (from Gent to the Rupel) and the estuarine zone (from Rupel to Vlissingen). In Fig. 9, the second column gives the total input flux from the upper river Scheldt and all tributaries. The two central columns indicate respectively the mass transfer between both areas and the



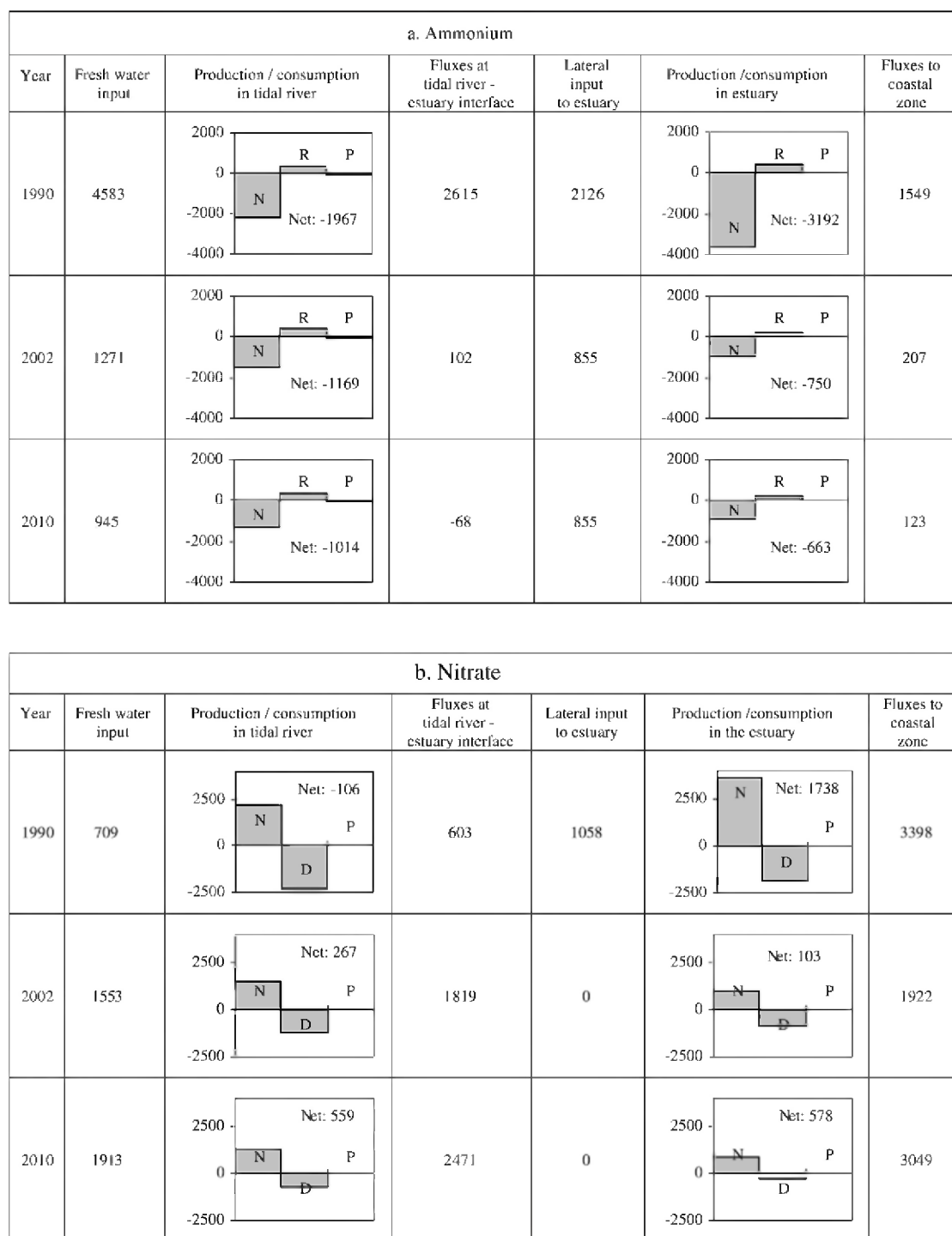


Fig. 9. Mass budget for (a) ammonium, (b) nitrate, (c) labile organic carbon and (d) oxygen. Processes: R=aerobic respiration; N=nitrification; D=denitrification; P=net primary production; M=phytoplankton mortality; A=oxygen transfer (aeration). Transport fluxes are positive seawards. All fluxes are given in  $\text{kmol day}^{-1}$ .

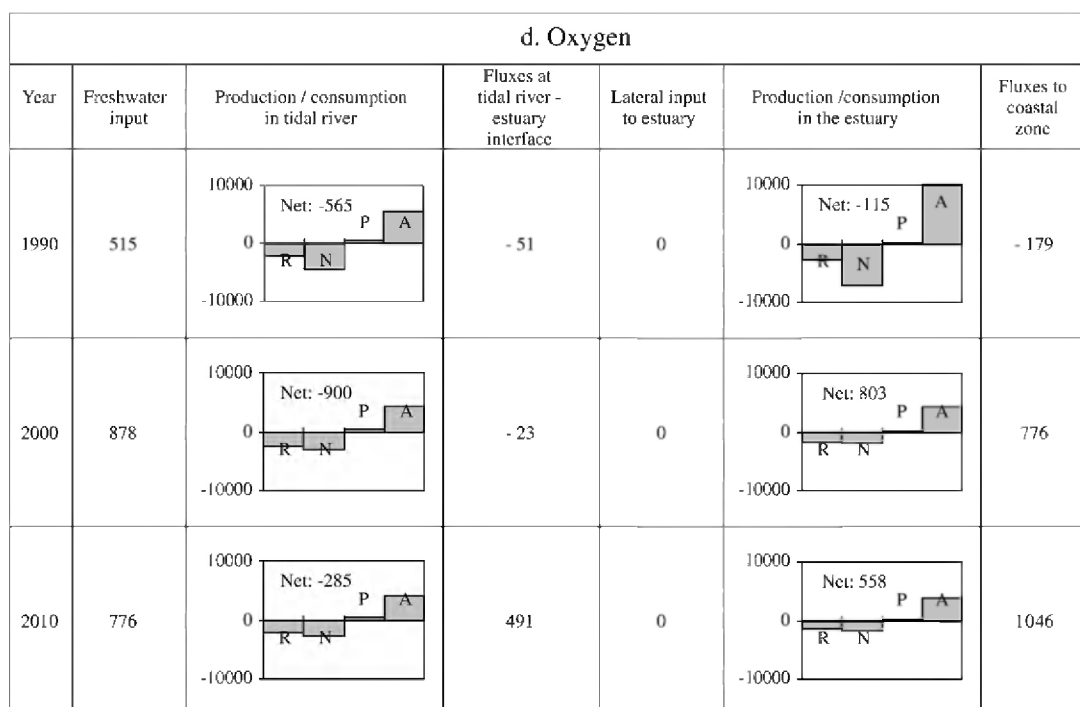
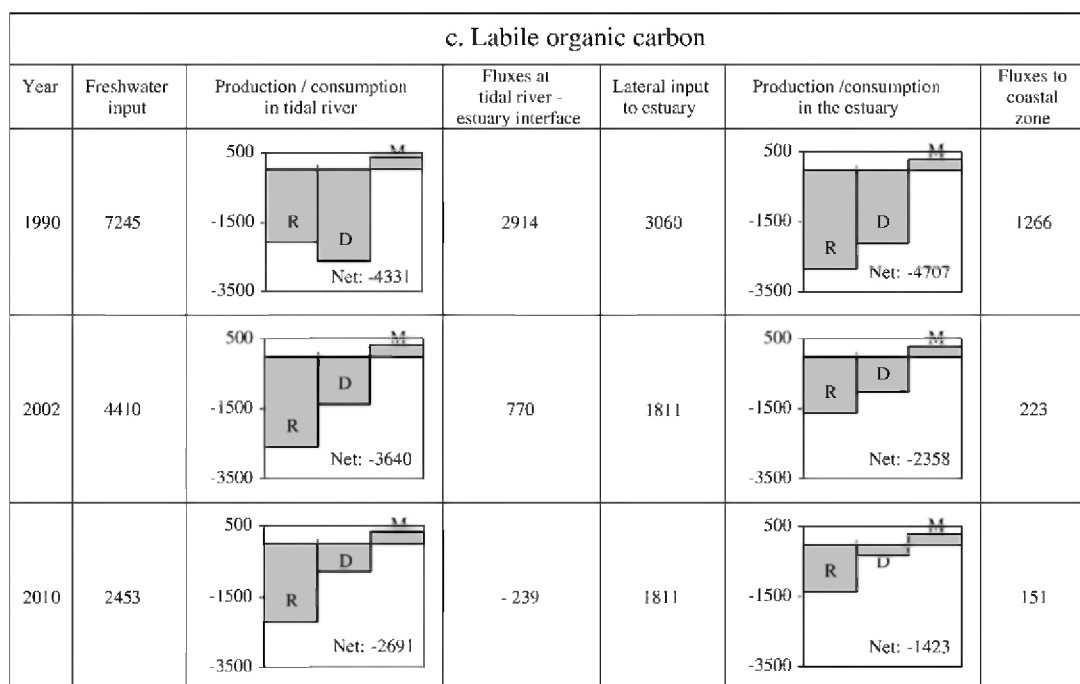


Fig. 9 (continued).

lateral inputs into the estuary, which originate from urban, industrial and agricultural sources. Finally, the left-most column gives the mass flux delivered to the coastal zone. The value inside each box corresponds to

the integrated process intensity occurring within the area. The distribution among the various processes involved is given by the bar graph, which includes aerobic (heterotrophic) respiration, nitrification,

denitrification, net phytoplankton production, phytoplankton mortality and oxygen transfer at the water/air interface. For the sake of clarity in the mass budgets, output fluxes from each box have been computed by difference to circumvent the short-term effects of mass variation in the estuary. Mass budgets are established by integration over the last two tidal cycles of the simulation (a time period of about 25 h). Yet, all our results are given in units of kmol per day.

The main features of these mass budgets can be synthesized as follows. (a) The estuarine system is clearly heterotrophic both in the upper (freshwater) and lower (brackish) parts. For all variables considered, the overall contribution of primary (phytoplankton) production is at least one order of magnitude lower than other processes involved. This situation is foreseen to persist in the future, although the rate of organic matter removal rate by heterotrophic respiration will considerably decrease. (b) The improvement in water quality arising from enhanced water sewerage and treatment is clearly demonstrated by the reduction of organic carbon fluxes, both within and at the boundaries of the estuarine compartments; in particular, a decrease in carbon flux is expected at the mouth of the estuary. (c) Concomitant with the expected decrease in ammonium supply, the relative importance of nitrification on the oxygen consumption will continue to decrease, although it will

remain comparatively as important as heterotrophic respiration. (d) Denitrification, which was in the past an important metabolic pathway of organic carbon and nitrate consumption in the estuary, will have its contribution considerably reduced in the future. The improvement in wastewater treatment, which leads to better redox conditions in the vicinity of Antwerp, could thus conduct to a worsening in terms of nitrogen export to the coastal zone. This situation, which had already been anticipated (Billen, 1990), can now be quantified with our model of the Scheldt continuum. (e) The similarity in integrated process intensities predicted for the tidal river (left bar graphs, Fig. 9) and the estuary (right bar graphs, Fig. 9) is striking: a number of transformation processes induce very comparable mass fluxes in both areas, although their geometry (volume, surface) differ widely and their freshwater residence time vary by 1 to 2 orders of magnitude. This result confirms the increasing importance of the tidal river on the overall biogeochemical behaviour of the Scheldt continuum. Accordingly, more research and monitoring efforts should be devoted in the future to the study of this area.

## 6. Conclusions

A two-dimensional, nested-grid model has been applied to the river–estuarine–coastal zone continuum

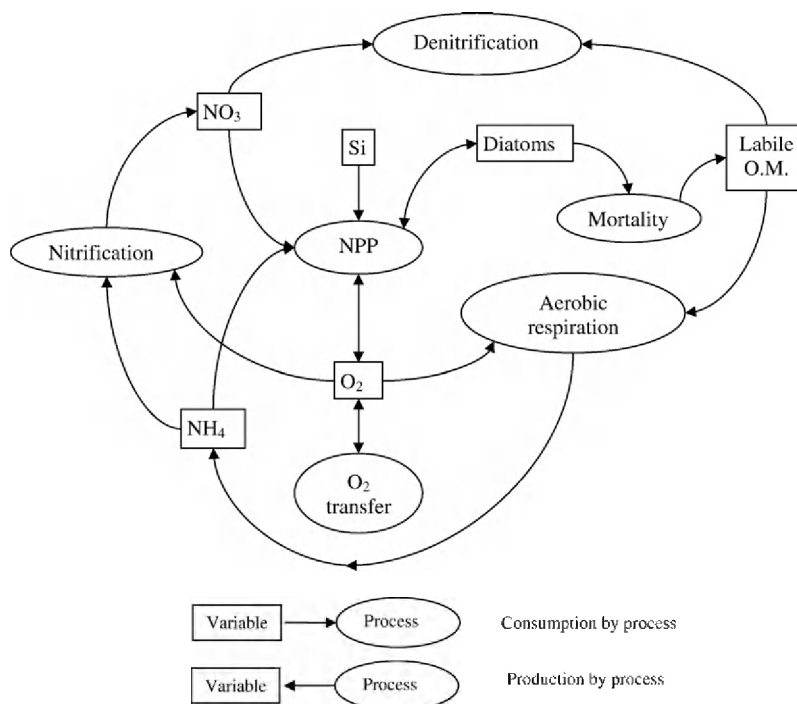


Fig. I.1. (Annex I) Sketch of the reaction network implemented in the model.

of the Scheldt, a system of particularly complex morphology and hydrodynamics. The reaction network for C, N, O<sub>2</sub> and Si was implemented in the MIKE 21-ECO Lab simulation environment (Fig. 1.1). Results obtained for average summer conditions show that our model captures the dominant features of the biogeochemical behaviour along the estuary and tidal river. The integrated modelling approach highlights the determining role of the spatio-temporal variability in residence time, depth, surface area and volume, on the biogeochemical dynamics. It also reveals that, despite widely varying length and time scales, the integrated transformation processes and fluxes are of comparable magnitude within each of the coupled sub-systems (river–estuary).

The dynamic coupling between the various modelled areas provides the proper framework to assess the impact of anthropogenic perturbations on water quality and to quantify export fluxes to the coastal zone. To advance further our understanding of the biogeochemical dynamics within the river–estuary environment, including its effect on coastal eutrophication, far better quantification of input fluxes at the system boundaries is needed. To carry accurate long-term transient simulations along the river–estuary–coastal zone system, a broad spectrum of temporal fluctuations should indeed be resolved, from daily to inter-seasonal variations in river discharge and water composition. Improved data acquisition strategies should thus be designed to avoid lack of sample representativeness and aliasing in data collection.

## Acknowledgments

We would like to thank Xavier Desmit (ULB) and Sandra Arndt (UU) for their collaboration during the set up and validation of the model. We also are indebted to two anonymous reviewers for their judicious remarks and fruitful suggestions. Numerous field data have been made available thanks to the OMES program funded by the Flemish regional authorities. This work has been partly funded by the EU project EUROTROPH (EVK3-CT-2000-00040) and by the Belgian Federal Office for Scientific, Technical and Cultural Affairs under the SISCO project (EV/11/17A).

## Appendix A

(1) *Net Primary Production* (NPP) by diatoms (dia) is the fraction of the vertically averaged gross primary production (GPP) which is not used for respiration

associated with growth and maintenance, or for cellular excretion (Desmit et al., 2005):

$$\text{NPP} [\mu\text{mol C m}^{-3} \text{ day}^{-1}] = \frac{\text{GPP}}{h} \cdot (1 - K_{\text{excret}}) \cdot (1 - K_{\text{growth}}) - k_{\text{maint}} \cdot \text{dia} \quad (\text{I.1})$$

where  $h$  is the water depth,  $K_{\text{excret}}$  and  $K_{\text{growth}}$  are the excretion and growth constants and  $k_{\text{maint}}$  is the specific maintenance respiration rate.

The vertically integrated GPP is calculated following the method described in Appendix B. A Michaelis–Menten factor incorporating the possible limitation of phytoplankton growth by silica (Si) has been added:

$$\text{GPP} [\mu\text{mol C m}^{-2} \text{ day}^{-1}] = \frac{P_{\text{max}}^{\text{B}} \text{dia}}{K_{\text{D}}} \cdot \frac{\text{Si}}{\text{Si} + K_{\text{m, Si}}} \cdot \left( f \left( \frac{I_0 \cdot \alpha}{P_{\text{max}}^{\text{B}}} \right) - f \left( \frac{I_{\text{bottom}} \cdot \alpha}{P_{\text{max}}^{\text{B}}} \right) + \log \left( \frac{I_0}{I_{\text{bottom}}} \right) \right) \quad (\text{I.2})$$

where  $K_{\text{m, Si}}$  is the half-saturation constant for Si,  $f$  is the piecewise definition of the Gamma function (Eq. (II.8)), and  $K_{\text{D}}$  is the light extinction coefficient in the water column, expressed as a linear regression of the suspended particulate matter concentration (SPM):

$$K_{\text{D}} [\text{m}^{-1}] = K_{\text{D1}} + K_{\text{D2}} \cdot \text{SPM}(S) \quad (\text{I.3})$$

SPM concentrations are estimated by nonlinear regression of salinity values  $S$  in the estuary:

$$\text{SPM} [\text{mg l}^{-1}] = 90 - (0.0749 \cdot S^2 - 0.2194 \cdot S + 1.4379) \quad (\text{I.4})$$

This approach, similar to the one followed by Soetaert and Herman (1993) in the MOSES model, only approximates the seaward decline of the mean SPM content in the water column and does not account for its variation in the freshwater part. It is however sufficient for the purpose of the present study. A more detailed description would require the use of an advanced model of sediment dynamics, which is beyond the scope of this work.

The concentration of NH<sub>4</sub> (nh4) is used to determine the relative proportion of the primary production sustained by nitrate and ammonium, respectively:

$$\text{NPP}_{\text{nh4}} = \text{fact}_{\text{nh4}} \cdot \text{NPP} \quad (\text{I.5})$$

$$\text{NPP}_{\text{no3}} = (1 - \text{fact}_{\text{nh4}}) \cdot \text{NPP} \quad (\text{I.6})$$



with

$$\text{fact}_{\text{nh4}} = \frac{\text{nh4}}{\text{nh4} + 10} \quad (\text{I.7})$$

The consumption of nitrogen species and silica is assumed directly proportional to the NPP, using typical molar Redfield ratios for N (redfieldN) and Si (redfieldSi).

(2) *Phytoplankton mortality* (phy\_mort) follows a first-order rate law with respect to the diatom concentrations (dia):

$$\text{phy\_mort} [\mu\text{M C day}^{-1}] = k_{\text{mortality}} \cdot \text{dia} \quad (\text{I.8})$$

with  $k_{\text{mortality}}$  as the first-order rate constant.

(3) *Aerobic degradation* (aer\_deg) is represented by a double Michaelis–Menten functional dependency with respect to labile organic matter (ch2o) and dissolved oxygen (o2), respectively:

$$\text{aer\_deg} [\mu\text{M C} \cdot \text{day}^{-1}] = k_{\text{ox}} \cdot \frac{\text{ch2o}}{\text{ch2o} + K_{\text{m, ch2o}}} \cdot \frac{\text{o2}}{\text{o2} + K_{\text{m, o2}}} \quad (\text{I.9})$$

where  $k_{\text{ox}}$  is the maximum rate constant of aerobic degradation;  $K_{\text{m, o2}}$  and  $K_{\text{m, ch2o}}$  are the half-saturation constants for  $\text{O}_2$  and labile O.M.

(4) *Denitrification* (denit) is modeled according to:

$$\text{denit} [\mu\text{M C day}^{-1}] = k_{\text{denit}} \cdot \frac{\text{ch2o}}{\text{ch2o} + K_{\text{m, ch2o}}} \cdot \frac{\text{no3}}{\text{no3} + K_{\text{m, no3}}} \cdot \frac{\text{Kin}_{\text{o2}}}{\text{o2} + \text{Kin}_{\text{o2}}} \quad (\text{I.10})$$

where  $k_{\text{denit}}$  is the maximum rate constant of denitrification and  $K_{\text{m, no3}}$  is the Michaelis–Menten constant for  $\text{NO}_3$ . The last term on the right hand side parameterizes the effect of oxygen inhibition on denitrification.

(5) *Nitrification* (nitrif) is modeled as a single-step process using a double Michaelis–Menten term with respect to  $\text{NH}_4$  and  $\text{O}_2$ :

$$\text{nitrif} [\mu\text{M N day}^{-1}] = k_{\text{nitrif}} \cdot \frac{\text{nh4}}{\text{nh4} + K_{\text{m, nh4}}} \cdot \frac{\text{o2}}{\text{o2} + K_{\text{m, o2}}} \quad (\text{I.11})$$

where  $k_{\text{nitrif}}$  is the maximum rate constant of nitrification,  $K_{\text{m, nh4}}$  and  $K_{\text{m, o2}}$  are the Michaelis–Menten constants for  $\text{NH}_4$  and  $\text{O}_2$ , respectively.

Table I.1

Parameter values of the reaction network

Name	Description	Value	Unit
$k_{\text{ox}}$	Aerobic degradation rate constant	25	$\mu\text{M C day}^{-1}$
$k_{\text{denit}}$	Denitrification rate constant	17	$\mu\text{M C day}^{-1}$
$k_{\text{nitrif}}$	Nitrification rate constant	13	$\mu\text{M N day}^{-1}$
$K_{\text{m, ch2o}}$	Half-saturation constant for organic matter	60	$\mu\text{M C}$
$K_{\text{m, o2}}$	Half-saturation constant for oxygen	15	$\mu\text{M O}_2$
$K_{\text{m, no3}}$	Half-saturation constant for nitrate	45	$\mu\text{M N}$
$K_{\text{m, nh4}}$	Half-saturation constant for ammonium	100	$\mu\text{M N}$
$K_{\text{m, Si}}$	Half-saturation constant for silica	20	$\mu\text{M Si}$
$\text{Kin}_{\text{o2}}$	Inhibition constant for denitrification	50	$\mu\text{M O}_2$
$K_{\text{D1}}$	Background extinction coefficient	1.3	$\text{m}^{-1}$
$K_{\text{D2}}$	Specific attenuation of suspended matter	0.06	$\text{l mg}^{-1} \text{m}^{-1}$
$\alpha$	Photosynthetic efficiency	0.025	$\text{m}^2 \text{s day}^{-1} \mu\text{E}^{-1}$
$P_{\text{max}}^{\text{B}}$	Maximum specific photosynthetic rate	10	$\text{day}^{-1}$
$k_{\text{maint}}$	Maintenance constant	0.08	$\text{day}^{-1}$
$K_{\text{growth}}$	Growth constant	0.3	–
$K_{\text{excretion}}$	Excretion constant	0.03	–
$k_{\text{mortality}}$	Mortality rate constant	0.06	$\text{day}^{-1}$
redfieldN	Redfield ratio for nitrogen	6.6	$\text{mol C} (\text{mol N})^{-1}$
redfieldSi	Redfield ratio for silica	5	$\text{mol C} (\text{mol Si})^{-1}$

(6) *Exchange of gaseous oxygen* (reaer) between the water column and the air is proportional to the departure from the saturation concentration in water, o2sat:

$$\text{reaer} [\mu\text{M O}_2 \text{ day}^{-1}] = \text{vp} \cdot (\text{o2sat} - \text{o2}) \quad (\text{I.12})$$

The saturation concentration depends on both temperature and salinity. The piston velocity, vp, is a function of current velocity, wind speed, Schmidt number and molecular diffusion of dissolved oxygen. See Vanderborght et al. (2002) for a detailed formulation of vp.

All constants used in the model, together with their numerical values and units, are listed in Table I.1.

## Appendix B

Platt equation describes phytoplankton Gross Primary Production (GPP) as a function of light intensity (Platt et al., 1980). With the assumption that the light profile decreases exponentially in the water column,

an expression for the depth distribution of GPP is obtained:

$$\text{GPP}(z) = P_{\max}^B \cdot \text{dia} \cdot \left( 1 - \exp\left(-\frac{\alpha \cdot I_0 \cdot \exp(-K_D \cdot z)}{P_{\max}^B}\right) \right) \quad (\text{II.1})$$

where  $P_{\max}^B$  is the maximum specific photosynthetic rate, dia is the concentration of phytoplankton biomass,  $\alpha$  is the photosynthetic efficiency,  $I_0$  is the solar radiation on the water surface,  $K_D$  is the light extinction coefficient, and  $z$  is the depth below the water surface.

The vertically integrated GPP is calculated by integrating Eq. (II.1) over the whole water depth,  $h$ :

$$\begin{aligned} \text{GPP} &= \int_{z=0}^{z=h} \text{GPP}(z) \cdot dz \\ &= \int_{z=0}^{z=h} P_{\max}^B \cdot \text{dia} \cdot \left( 1 - \exp\left(-\frac{\alpha \cdot I_0 \cdot \exp(-K_D \cdot z)}{P_{\max}^B}\right) \right) \cdot dz \end{aligned} \quad (\text{II.2})$$

where dia and  $K_D$  have been assumed constant along the water column. This integral is of the form  $\int_a \cdot \exp(b \cdot \exp(c \cdot x)) \cdot dx$  whose primitive requires to be expressed with special functions. By changing the integration variable from depth below water surface,  $z$ , to light intensity,  $I$ , we have that

$$\text{GPP} = \frac{P_{\max}^B \cdot \text{dia}}{K_D} \int_{I_{\text{bottom}}}^{I_0} \frac{1 - \exp\left(-\alpha \cdot \frac{I}{P_{\max}^B}\right)}{I} dI \quad (\text{II.3})$$

where  $I_{\text{bottom}}$  is the light intensity at  $z=h$ . Integration of Eq. (II.3) leads to the following expression:

$$\begin{aligned} \text{GPP} &= \frac{P_{\max}^B \cdot \text{dia}}{K_D} \left( \Gamma\left(0, \frac{I_0 \cdot \alpha}{P_{\max}^B}\right) - \Gamma\left(0, \frac{I_{\text{bottom}} \cdot \alpha}{P_{\max}^B}\right) \right. \\ &\quad \left. + \log\left(\frac{I_0}{I_{\text{bottom}}}\right) \right) \end{aligned} \quad (\text{II.4})$$

where  $\Gamma(0, x)$  denotes a special case of the incomplete gamma function, which corresponds to the exponential integral through the equation:

$$\Gamma(0, x) = E_1(x) \quad x > 0 \quad (\text{II.5})$$

This exponential integral can be approximated by fast converging piecewise definition (e.g. Press et al., 1992), depending on the value of the argument  $x$ :

$$E_1(x) = \begin{cases} -(\ln(x) + \gamma) - \left( \frac{-x}{1!} + \frac{(-x)^2}{2 \cdot 2!} + \frac{(-x)^3}{3 \cdot 3!} + \frac{(-x)^4}{4 \cdot 4!} + \dots \right), & 0 < x \leq 1 \\ e^{-x} \left( \frac{1}{x+1} - \frac{1}{x+3} + \frac{2^2}{x+5} - \frac{3^2}{x+7} + \dots \right), & x > 1 \end{cases} \quad (\text{II.6})$$

where  $\gamma$  is Euler's constant and the expression in parenthesis for  $x > 1$  represents a continued fraction. For the depth integrated GPP, a five-terms approximation of  $E_1(x)$  leads to an error of the order of  $10^{-14}$ :

$$\text{GPP} \approx \frac{P_{\max}^B \cdot \text{dia}}{K_D} \cdot \left( f\left(\frac{I_0 \cdot \alpha}{P_{\max}^B}\right) - f\left(\frac{I_{\text{bottom}} \cdot \alpha}{P_{\max}^B}\right) + \log\left(\frac{I_0}{I_{\text{bottom}}}\right) \right) \quad (\text{II.7})$$

where:

$$f(x) = \begin{cases} -(\log(x) + \gamma) - (-x + x^2/4 - x^3/18 + x^4/96 - x^5/600), & 0 < x \leq 1 \\ \exp(-x) \cdot \{1/(x+1) - 1/(x+3) - 4/(x+5) - 9/(x+7) - 16/(x+9)\}, & x > 1 \end{cases} \quad (\text{II.8})$$

## References

- Abbott, M.B., 1979. Computational Hydraulics: Elements of the Theory of Free Surface Flows. Pitman, London.
- Arndt, S., Vanderborght, J.P., Regnier, P., in press. Phytoplankton growth response to physical forcing in a macrotidal estuary: coupling hydrodynamics, sediment transport and biogeochemistry. Journal of Geophysical Research—Oceans.
- AWZ, 2003. Westerschelde: Monding-Rupel. Ministerie van de Vlaamse Gemeenschap, Departement Leefmilieu en Infrastructuur, Administratie Waterwegen en Zeewezen, Afdeling Kust. (Chart with 12 maps).
- Billen, G., 1990. N-budget of the major rivers discharging into the continental coastal zone of the North Sea: the nitrogen paradox. In: Lancelot, C., Billen, G., Barth, H. (Eds.), Eutrophication and Algal Blooms in North Sea Coastal Zones, The Baltic and Adjacent Areas: Predictions and Assessment of Prevention Actions. Water Pollution Research Report, vol. 12, p. 172.
- Billen, G., Lancelot, E., De Becker, E., Servais, P., 1988. Modelling microbial processes (phyto- and bacterioplankton) in the Schelde estuary. Hydrobiological Bulletin 22, 43–55.
- Billen, G., Garnier, J., Ficht, A., Cun, C., 2001. Modeling the response of water quality in the Seine River estuary to human activity in its watershed over the last 50 years. Estuaries 24, 977–993.
- Billen, G., Garnier, J., Rousseau, V., 2005. Nutrient fluxes and water quality in the drainage network of the Scheldt basin over the last 50 years. Hydrobiologia 540, 47–67.
- Desmit, X., Vanderborght, J.P., Regnier, P., Wollast, R., 2005. Control of primary production by physical forcing in strong tidal estuaries. Biogeosciences 2, 205–218.
- Ekebjærg, L., Justesen, P., 1991. An explicit scheme for advection–diffusion modelling in two dimensions. Computer Methods in Applied Mechanics and Engineering 88, 287–297.
- Fischer, H., List, E.J., Koh, C.R., Imberger, J., Brooks, N.H., 1979. Mixing in Inland and Coastal Waters. Academic Press.
- Garnier, J., Billen, G., Coste, M., 1995. Seasonal succession of diatoms and Chlorophyceae in the drainage network of the Seine River: observations and modeling. Limnology and Oceanography 40, 750–765.
- IRM, 2004. In: Malcorps, H. (Ed.), Observations climatologiques — Bulletin mensuel de l'Institut Royal Météorologique de Belgique. Institut Royal Météorologique de Belgique—Royal Meteorological Institute of Belgium, Bruxelles.
- Jay, D.A., Uncles, R.J., Largier, J., Geyer, W.R., Vallino, J., Boynton, W.R., 1997. A review of recent developments in estuarine scalar flux estimation. Estuaries 20, 262–280.

- Jensen, H.R., Møller, J.S., Rasmussen, B., 2002. Operational hydrodynamical model of the Danish waters, Danish Program for monitoring the Water Environment. In: Flemming, N.C., Vallega, S., Pinardi, N., Behrens, H.W.A., Manzella, G., Prandle, D., Stel, J.H. (Eds.), *Operational Oceanography: Implementation at the European and Regional scales*. Elsevier Oceanography Series, vol. 66. Elsevier, Amsterdam.
- Lancelot, C., Rousseau, V., Billen, G., Van Eckhout, D., 1997. Coastal eutrophication of the Southern Bight of the North Sea: assessment and modelling. In: Ozsoy, E., Mikaelyan, A. (Eds.), *Sensitivity of North Sea, Baltic Sea and Black Sea to anthropogenic and climatic changes*. NATO-ASI Series, vol. 2.27, pp. 439–454.
- Lebo, M.E., Sharp, J.H., 1992. Modeling phosphorus cycling in a well-mixed coastal plain estuary. *Estuarine, Coastal and Shelf Science* 35, 235–252.
- Loder, T.C., Reichard, R.P., 1981. The dynamics of conservative mixing in estuaries. *Estuaries* 4, 64–69.
- Maris, T., Van Damme, S., Meire, P. (Red.), 2004. Onderzoek naar de gevolgen van het Sigmaphan, baggeractiviteiten en havenuitbreiding in de Zeeschelde op het milieu. Geïntegreerd eindverslag van het onderzoek verricht in 2003. Universiteit Antwerpen, Antwerpen (in Dutch).
- Muylert, K., Sabbe, K., Vijverman, W., 2000. Spatial and temporal dynamics of phytoplankton communities in a freshwater tidal estuary. *Estuarine, Coastal and Shelf Science* 50, 673–687.
- Officer, C.B., Lynch, D.R., 1981. Dynamics of mixing in estuaries. *Estuarine, Coastal and Shelf Science* 12, 525–533.
- O’Kane, J.P., Regnier, P.A., 2003. A mathematically transparent low-pass filter for tidal estuaries. *Estuarine, Coastal and Shelf Science* 57, 593–603.
- Peters, J.J., Sterling, A., 1976. Hydrodynamique et transport de sédiments de l’estuaire de l’Escaut. *Projet Mer*, Vol. 10. Service de Programmation de la Politique Scientifique, Bruxelles, Belgium, pp. 1–95 (in French).
- Platt, T., Gallegos, C.L., Harrison, W.G., 1980. Photoinhibition of photosynthesis in natural assemblages in marine phytoplankton. *Journal of Marine Research* 38, 687–701.
- Press, W.H., Teukolsky, S.A., Vetterling, W.T., Flannery, B.P., 1992. *Numerical Recipes in Fortran 77*. The Art of Scientific Computing. Cambridge University Press, Cambridge.
- Proctor, R., Holt, J., Harris, J., Tappin, A., Boorman, D., 2000. Modelling the Humber estuary catchment and coastal zone. In: Spaulding, M., Butler, H.L. (Eds.), *Estuarine and Coastal Modelling: Proceedings of the 6th International Conference*. American Society of Civil Engineers, pp. 1259–1274.
- Regnier, P., 1997. Long-term fluxes of reactive species in strong tidal estuaries: model development and application to the Western Scheldt estuary. Ph.D. Thesis, Université Libre de Bruxelles, Belgium.
- Regnier, P., O’Kane, J.P., 2004. On the mixing processes in estuaries: the fractional freshwater method revisited. *Estuaries* 27, 571–582.
- Regnier, P., Steefel, C.I., 1999. A high resolution estimate of the inorganic nitrogen flux from the Scheldt estuary to the coastal North Sea during a nitrogen-limited algal bloom, spring 1995. *Geochimica Cosmochimica Acta* 63, 1359–1374.
- Regnier, P., Wollast, R., Steefel, C.I., 1997. Long term fluxes of reactive species in macrotidal estuaries: estimates from a fully transient, multi-component reaction transport model. *Marine Chemistry* 58, 127–145.
- Regnier, P., Mouchet, A., Wollast, R., Rondy, F., 1998. A discussion of methods for estimating residual fluxes in strong tidal estuaries. *Continental Shelf Research* 18, 1543–1571.
- SAWES, 1991. Waterkwaliteitsmodel Schelde-estuarium. WL-rapport T257, Waterloopkundig Laboratorium, Delft, The Netherlands (in Dutch).
- Smagorinsky, J., 1963. General circulation experiments with the primitive equations. *Monthly Weather Review* 91, 99–164.
- Soetaert, K., Herman, P.M.J., 1993. MOSES-model of the Scheldt estuary. Ecosystem model development under SENECA. Report of the NIOO (Netherlands Institute for Ecology), Centre for Marine and Estuarine Ecology, Yerseke (The Netherlands).
- Soetaert, K., Herman, P.M.J., 1995a. Nitrogen dynamics in the Westerschelde estuary (SW Netherlands) estimated by means of the ecosystem model MOSES. *Hydrobiologia* 311, 225–246.
- Soetaert, K., Herman, P.M.J., 1995b. Carbon flows in the Westerschelde estuary (The Netherlands) evaluated by means of an ecosystem model (MOSES). *Hydrobiologia* 311, 247–266.
- Soetaert, K., Middelburg, J.J., Heip, C., Meire, P., Van Damme, S., Maris, T., 2006. Long-term change in dissolved inorganic nutrients in the heterotrophic Scheldt estuary (Belgium, The Netherlands). *Limnology and Oceanography* 51, 409–423.
- Tappin, A.D., 2002. An examination of the fluxes of nitrogen and phosphorus in temperate and tropical estuaries: current estimates and uncertainties. *Estuarine, Coastal and Shelf Science* 55, 885–901.
- Tappin, A.D., Harris, J.R.W., Uncles, R.J., 2003. The fluxes and transformations of suspended particles, carbon and nitrogen in the Humber estuarine system (UK) from 1994 to 1996: results from an integrated observation and modelling study. *Science of the Total Environment* 314–316, 665–713.
- Thouvenin, B., Le Hir, P., Romana, L.A., 1994. Dissolved oxygen model in the Loire Estuary. In: Dyer, K.R., Orth, R.J. (Eds.), *Changes in Fluxes in Estuaries: Implications from Science to Management*. Olsen and Olsen, Fredensborg, pp. 169–178.
- Van Damme, S., Meire, P., Maeckelberghe, H., Verdier, M., Bourgoing, L., Tavemiers, E., Ysebaert, T., Wattel, G., 1995. De waterkwaliteit van de Zeeschelde: evolutie in de voorbije dertig jaar. *Water* 85, 244–256 (in Dutch).
- Vanderborght, J.P., Wollast, R., Loijens, M., Regnier, P., 2002. Application of a transport-reaction model to the estimation of biogas fluxes in the Scheldt estuary. *Biogeochemistry* 59, 207–237.
- VMM, 2003. Waterkwaliteit - Lozingen in het water 2002. Vlaamse Milieumaatschappij, Erembodegem, Belgium (in Dutch).
- WKL, 1966. Stormvloed op de Schelde. Report nr 4, Waterbouwkundig Laboratorium, Borgerhout, Belgium (in Dutch).
- Wollast, R., 1978. Modelling of biological and chemical processes in the Scheldt estuary. In: Nihoul, J.C.J. (Ed.), *Hydrodynamics of Estuaries and Fjords*. Elsevier Oceanography Series, Amsterdam, vol. 23, pp. 63–78.
- Wollast, R., 1988. The Scheldt estuary. In: Salomons, W., Bayne, B.L., Duursma, E.K., Förstner, U. (Eds.), *Pollution of the North Sea: An Assessment*. Springer-Verlag, Berlin, pp. 183–193.
- Wollast, R., 2003. Biogeochemical processes in estuaries. In: Wefer, G., Lamy, F., Mantoura, F. (Eds.), *Marine Science Frontiers for Europe*. Springer-Verlag, Berlin, pp. 61–77.